

# Fast-activating cation channel in barley mesophyll vacuoles. Inhibition by calcium

Liubov I. Tikhonova<sup>†</sup>, Igor I. Pottosin<sup>†</sup>, Karl-Josef Dietz and Gerald Schönknecht\*

Lehrstuhl Botanik I, Universität Würzburg, Mittlerer Dallenbergweg 64, D-97082 Würzburg, Germany

## Summary

In contrast to the vacuolar ion channels which are gated open by an increase of cytosolic  $\text{Ca}^{2+}$  the vacuolar ion currents at resting cytosolic  $\text{Ca}^{2+}$  are poorly explored. Therefore, this study was performed to investigate the properties of the so-called fast-activating vacuolar (FV) current which dominates the electrical characteristics of the tonoplast at physiological free  $\text{Ca}^{2+}$  concentrations. Patch-clamp measurements were performed on whole barley (*Hordeum vulgare*) mesophyll vacuoles and on excised tonoplast patches. Single ion channels were identified, which, based on their selectivity, activation kinetics,  $\text{Ca}^{2+}$ - and voltage-dependence, carry the whole-vacuole FV current. Reversal potential determinations indicated a  $\text{K}^+$  over  $\text{Cl}^-$  permeability ratio of about 30. Both inward and outward whole-vacuole currents as well as the activity of single FV channels were inhibited by an increase of cytosolic  $\text{Ca}^{2+}$ , with a  $K_d \approx 6 \mu\text{M}$ . At physiological vacuolar  $\text{Ca}^{2+}$  activities, the FV channel is an outward-rectifying potassium channel. The FV channel was activated in less than a few milliseconds both by negative and positive potential steps, having a minimal activity that is 40 mV negative of the  $\text{K}^+$  equilibrium potential. It is proposed that transport of  $\text{K}^+$  through this cation channel controls the electrical potential difference across the tonoplast.

## Introduction

There are two major ion currents in plant vacuoles, the so-called slow-activating (SV) and fast-activating (FV) vacuolar currents. The SV channel is activated by cytosolic free  $\text{Ca}^{2+}$  concentrations in the micromolar range and by positive tonoplast potentials relative to the cytoplasm (Hedrich and Neher, 1987; Reifarth *et al.*, 1994; Schulz-Lessdorf and Hedrich, 1995). The FV current is activated by low ( $< 1 \mu\text{M}$ ) cytosolic free  $\text{Ca}^{2+}$  and by both positive and negative tonoplast potentials (Hedrich and Neher, 1987). Since the

discovery of the SV and FV currents (Hedrich and Neher, 1987; Hedrich *et al.*, 1986) a lot of work has been done towards the understanding of permeability characteristics, pharmacology, regulation and possible physiological role of the SV channel (Allen and Sanders, 1995; Hedrich and Kurkdjan, 1988; Hedrich *et al.*, 1988; Pantoja *et al.*, 1992a, b; Reifarth *et al.*, 1994; Schulz-Lessdorf and Hedrich, 1995; Ward and Schroeder, 1994; Weiser and Bentrup, 1993). At the same time, much less attention was paid to the FV current, which appears to dominate at physiological conditions, low cytosolic  $\text{Ca}^{2+}$  and voltages close to the resting tonoplast potential. Therefore, we studied the fast activating ion current in barley mesophyll vacuoles, giving primary attention to its dependence on free cytosolic and vacuolar  $\text{Ca}^{2+}$  concentrations. We were able to identify single ion channels which, based on their activation kinetics, voltage- and  $\text{Ca}^{2+}$  dependence, and  $\text{K}^+/\text{Cl}^-$  selectivity, are responsible for the whole-vacuole FV current.

## Results

### Dependence of whole vacuolar currents on cytosolic calcium

Whole-vacuole currents were recorded with 2 mM  $\text{Ca}^{2+}$  inside the vacuole, and the free  $\text{Ca}^{2+}$  concentration at the cytosolic side was changed from  $< 1 \text{ nM}$  (referred to as 0  $\text{Ca}^{2+}$ ) to 0.5 mM. The instantaneous component of the whole-vacuole current under these conditions displayed an outward rectification as shown in Figure 1(a). There was large current flow at positive potentials (relative to the cytoplasm), i.e. efflux of cations from the cytoplasm into the vacuole or influx of anions from the vacuole into the cytoplasm. Increasing the cytosolic  $\text{Ca}^{2+}$  concentration from 0 to 5  $\mu\text{M}$  resulted in a twofold decrease of the outward rectifying instantaneous currents. It should be noted that the relative small instantaneous inward currents at 2 mM vacuolar  $\text{Ca}^{2+}$  also decreased at increasing cytosolic  $\text{Ca}^{2+}$  (Figure 1a). A further increase of cytosolic  $\text{Ca}^{2+}$  to 50  $\mu\text{M}$  resulted in a further decrease of the amplitude of the instantaneous currents, and in the activation of a slowly-activating vacuolar current at positive potentials above +50 mV. The amplitudes of the instantaneous currents were plotted as a function of the applied membrane voltage at different levels of cytosolic  $\text{Ca}^{2+}$  (Figure 1b). The resulting current–voltage ( $I/V$ ) relationships show that the amplitude of the current decreased proportionally over the whole voltage range with increasing cytosolic

Received 5 August 1996; revised 13 January 1997; accepted 12 February 1997.

\*For correspondence (fax +49 931 888 6158; e-mail gerald@botanik.uni-wuerzburg.de).

<sup>†</sup>Permanent address: Institute for Cell Biophysics, Russian Academy of Sciences, 142292 Pushchino, Moscow Region, Russia.

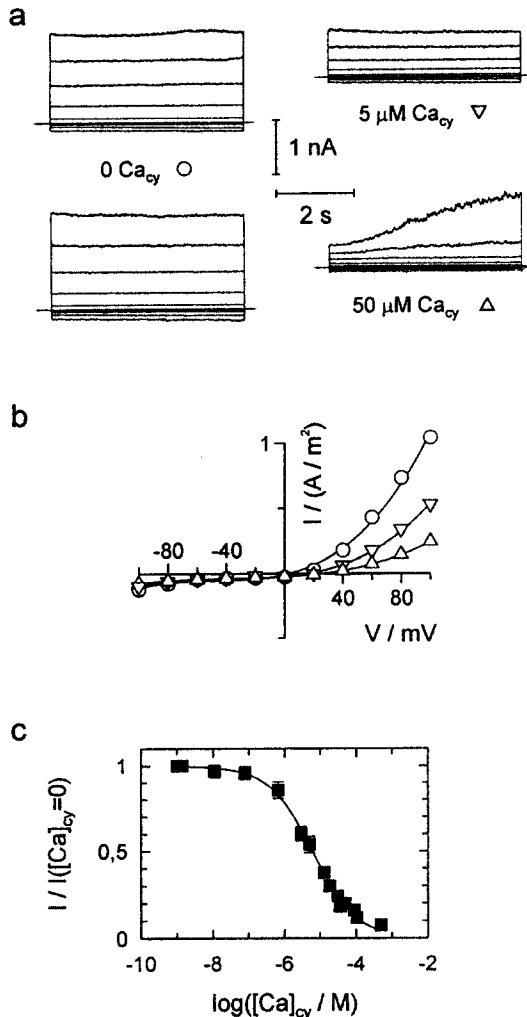


**Figure 1.** Effect of increasing cytosolic  $\text{Ca}^{2+}$  concentration on fast-activating vacuolar currents at 2 mM vacuolar  $\text{Ca}^{2+}$ .

(a) Whole-vacuolar currents ( $I$  in nA) at different levels of cytosolic  $\text{Ca}^{2+}$  ( $\text{Ca}_{\text{cy}}$ ). The measurements were performed in symmetrical 100 mM KCl. From a holding potential of 0 mV, the electrical potential across the tonoplast was changed for 4.9 s in 20 mV steps from  $-100$  to  $+100$  mV. At the beginning of the experiment (upper left), cytosolic  $\text{Ca}^{2+}$  was buffered to  $< 1$  nM by 5 mM EGTA ( $0 \text{ Ca}_{\text{cy}}$ ,  $\circ$ ). By bath perfusion, the external solution (cytoplasmic side) was changed to  $5 \mu\text{M}$  ( $\nabla$ ) and  $50 \mu\text{M}$  ( $\triangle$ ) free  $\text{Ca}^{2+}$ . At the end of the experiment, 90 min later and after perfusing 15 different  $\text{Ca}^{2+}$  concentrations, another measurement was performed at  $0 \text{ Ca}_{\text{cy}}$  (lower left). Vacuolar currents were digitized and filtered at 200 Hz. The capacitance of the vacuole in this experiment was 15 pF.

(b) The amplitude of the instantaneous vacuolar currents shown in (a) as a function of membrane voltage ( $V$  in mV) for three different cytosolic  $\text{Ca}^{2+}$  concentrations. Different symbols reflect different  $\text{Ca}^{2+}$  concentrations as in (a). The current amplitudes were normalized to the vacuolar membrane surface as calculated from the measured capacitance assuming a specific capacitance of  $0.01 \text{ F m}^{-2}$  and expressed in  $\text{A m}^{-2}$ . The solid lines are low-order polynomials fitted to the data.

(c) The dependence of fast vacuolar currents on the cytosolic  $\text{Ca}^{2+}$  concentration. With six separate vacuoles, up to 15 different cytosolic  $\text{Ca}^{2+}$  concentrations were applied (15 in three experiments, 5–8 in another three). Each data point gives the mean  $\pm$  SD (each concentration was measured with at least four different vacuoles). Whole-vacuolar currents at  $+100$  mV were normalized to the current at  $0 \text{ Ca}_{\text{cy}}$ . The data points were fitted by a Hill equation (solid line), yielding a Hill coefficient of  $0.70 \pm 0.026$  and  $\log(K_{\text{d}}) = -5.23 \pm 0.02$ , i.e.  $K_{\text{d}} = 5.9 \mu\text{M}$ .

$\text{Ca}^{2+}$  activities. The relative current amplitudes at  $+100$  mV were plotted as a function of the cytosolic  $\text{Ca}^{2+}$  activity in Figure 1(c). The blockage of the instantaneous currents by cytosolic  $\text{Ca}^{2+}$  could be described by a  $\text{Ca}^{2+}$  binding with an affinity of  $6 \mu\text{M}$  and a Hill coefficient of 0.7. At the end of each experiment, the  $0 \text{ Ca}^{2+}$  solution was returned to the measuring chamber. Even after more than one hour's perfusion, only a small rundown of the fast vacuole currents was detected, never exceeding 20% of the initial currents (Figure 1a).

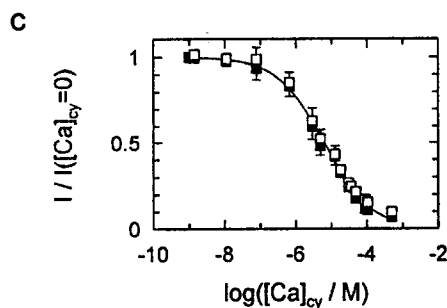
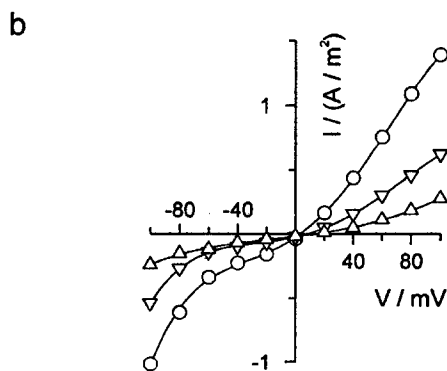
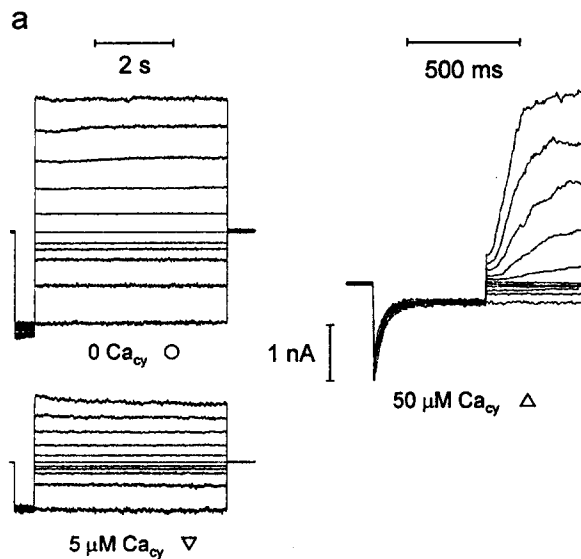
Outward rectification of the fast vacuolar current (Figure 1a and b) was observed with 2 mM  $\text{Ca}^{2+}$  in the vacuole and  $0 \text{ Ca}^{2+}$  in cytoplasm, under otherwise symmetrical ion conditions (100 mM KCl at the both membrane sides). As can be seen in Figure 2(a), with  $0 \text{ Ca}^{2+}$  on both sides of the tonoplast, the instantaneous currents had comparable amplitudes at positive and negative potentials. An increase of cytosolic  $\text{Ca}^{2+}$  decreased both the outward and the inward instantaneous currents. The  $I/V$  relationships of the instantaneous currents at different levels of cytosolic  $\text{Ca}^{2+}$  activity are displayed in Figure 2(b). The relative amplitudes of the fast activating current at  $+100$  and  $-100$  mV were plotted as a function of cytosolic free  $\text{Ca}^{2+}$  (Figure 2c). Both sets of data can be fitted by the same curve, with a  $K_{\text{d}}$  of  $6 \mu\text{M}$  and a Hill coefficient of 0.7.

We attempted to resolve the activation–deactivation kinetics of the fast vacuolar currents, but it was obviously faster than the time course which can be resolved by our measuring set-up. The half-rise times were less than 1 ms (data from 10 separate vacuoles).

#### Dependence of the whole-vacuole current on vacuolar calcium

To analyse the effect of vacuolar  $\text{Ca}^{2+}$  on the FV current in more detail, three intermediate vacuolar free  $\text{Ca}^{2+}$  concentrations, namely  $5 \mu\text{M}$ ,  $18 \mu\text{M}$  and  $50 \mu\text{M}$ , were examined. With  $0 \text{ Ca}^{2+}$  on the cytosolic side, the free  $\text{Ca}^{2+}$  concentration in the pipette filling solution was fixed to different levels, and 31 vacuoles were examined. The resulting  $I/V$  relationships of the instantaneous whole-vacuole current are shown in Figure 3(a). It can be seen that for up to  $50 \mu\text{M}$   $\text{Ca}^{2+}$  inside the vacuole, the outward current (at positive potentials) was unaffected, while with 2 mM  $\text{Ca}^{2+}$  in the vacuole, the outward current was decreased by 37% compared with  $0 \text{ Ca}^{2+}$  at  $+100$  mV. At the same time, even at  $5 \mu\text{M}$   $\text{Ca}^{2+}$ , there is a significant decrease of the inward current (at negative potentials). To describe the effect of vacuolar  $\text{Ca}^{2+}$  on the inward current quantitatively, the relative current at  $-100$  mV was plotted against the free  $\text{Ca}^{2+}$  concentration inside the vacuole (Figure 3b). The data points can be fitted assuming  $\text{Ca}^{2+}$  binding at the luminal side of the membrane, with a  $K_{\text{d}}$  for  $\text{Ca}^{2+}$  of  $14 \mu\text{M}$  and a Hill coefficient of 0.5. Despite this relative high  $\text{Ca}^{2+}$  binding

affinity from the vacuolar side, a small inward current remained even at millimolar  $\text{Ca}^{2+}$ . For instance, at 2 mM vacuolar  $\text{Ca}^{2+}$ , the inward current at  $-100$  mV had an amplitude of about 8% compared with 0  $\text{Ca}^{2+}$  (Figure 3b). This was significantly larger than the non-specific leak current, which was about  $-0.024$  A  $\text{m}^{-2}$  at  $-100$  mV as an average, or 3% of the maximum current. The leak current was estimated by linearly extrapolating the current measured with 2 mM  $\text{Ca}^{2+}$  inside the vacuole (Figure 3a) from



the high-resistance region around  $-40$  mV to more negative potentials.

#### Ion selectivity of the fast vacuolar current

Starting with symmetrical 100 mM KCl, we decreased the KCl concentration in the bath to 10 mM to determine the ion selectivity of the fast vacuolar current. The resulting  $I/V$  curves with 2 mM  $\text{Ca}^{2+}$  inside the vacuole (Figure 4a) and the  $I/V$  curves with 0  $\text{Ca}^{2+}$  at both membrane sides (Figure 4b) displayed the same reversal potentials. The 10-fold decrease of the KCl concentration shifted the reversal potential by 50 mV to more positive voltages. The reversal potential of about  $+50$  mV came close to the equilibrium potential for  $\text{K}^+$  of  $+56$  mV (after correcting for ion activities) suggesting a high  $\text{K}^+/\text{Cl}^-$  permeability ratio. This result indicates that the fast vacuolar current is carried by monovalent cations, although a small contribution of  $\text{Cl}^-$  cannot be ruled out. Accordingly, the 10-fold decrease of the KCl concentration in the bath resulted in a decrease of the outward current, i.e. the efflux of  $\text{K}^+$  from the bath into the vacuole. A threefold increase of the KCl concentration in the bath from 100 mM to 300 mM resulted in an increase of the outward current by about 35% at  $+100$  mV, as shown in Figure 4. Thus, the fast vacuolar current tended to saturate at some hundred millimoles of  $\text{K}^+$ . The slope conductance determined from the linear portion of  $I/V$  relationships for the outward whole vacuolar current was  $4.2 \pm 1.0$ ,  $12.6 \pm 0.6$ ,  $16.6 \pm 0.9$ ,  $23.3 \pm 0.2$ , and  $22.0 \pm 0.8$  S  $\text{m}^{-2}$  for 10, 30, 100, 300 and 1000 mM cytosolic  $\text{K}^+$ , respectively ( $n = 6, 2, 6, 3$  and 4 vacuoles). These data points were fitted assuming a Michaelis–Menten type of

**Figure 2.** Effect of increasing cytosolic  $\text{Ca}^{2+}$  concentration on fast-activating vacuolar currents at zero vacuolar  $\text{Ca}^{2+}$ .

(a) Whole-vacuolar currents ( $I$  in nA) at different levels of cytosolic  $\text{Ca}^{2+}$  ( $\text{Ca}_{\text{cy}}$ ). All experiments were performed in symmetrical 100 mM KCl and 0 Ca inside the vacuole. From a holding potential of 0 mV, the electrical potential across the tonoplast was first stepped to  $-100$  mV for 0.5 s to deactivate slow vacuolar channels, then the voltage was changed for 4.9 s in 20 mV steps from  $-100$  to  $+100$  mV. By bath perfusion, the external solution was changed from 0  $\text{Ca}_{\text{cy}}$  (O) to 5  $\mu\text{M}$  (▽) and 50  $\mu\text{M}$  (△) free  $\text{Ca}^{2+}$ . The whole-vacuolar currents at 50  $\mu\text{M}$   $\text{Ca}_{\text{cy}}$  are displayed on an expanded time scale. This shows that after the deactivation of SV channels by a  $-100$  mV pulse, the small instantaneous currents can unambiguously be separated from the slowly activating SV current. In this experiment, a vacuole with a capacitance of 17 pF was used.

(b) The amplitude of the instantaneous vacuolar currents shown in (a) as a function of membrane voltage ( $V$  in mV) for three different cytosolic  $\text{Ca}^{2+}$  concentration. Different symbols reflect different  $\text{Ca}^{2+}$  concentrations as in (a). The current amplitudes were normalized to the vacuolar membrane surface and expressed in A  $\text{m}^{-2}$ . Solid lines are low-order polynomials fitted to the data.

(c) The dependence of fast vacuolar currents on the cytosolic  $\text{Ca}^{2+}$  concentration. Whole-vacuolar currents were measured at  $-100$  mV (■) and at  $+100$  mV (□) and normalized to the current at 0  $\text{Ca}_{\text{cy}}$ . Each data point represents the mean  $\pm$  SD of three separate vacuoles. The data points of both data sets were fitted simultaneously by a Hill equation, yielding a Hill coefficient of  $0.66 \pm 0.02$  and  $\log(K_d) = -5.20 \pm 0.02$ , i.e.  $K_d = 6.3$   $\mu\text{M}$ .

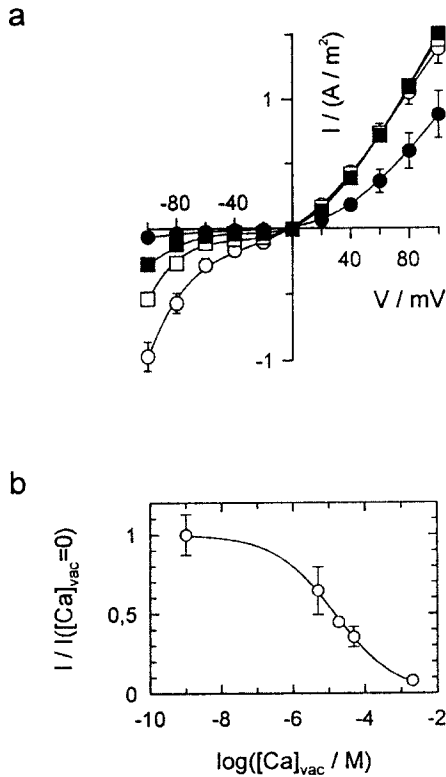


**Figure 3.** Inhibition of the fast-activating inward current by vacuolar calcium. (a) Whole-vacuole  $I / V$  relationships at different vacuolar free  $Ca^{2+}$  concentrations. The concentration of KCl was 100 mM at both membrane sides. Cytosolic  $Ca^{2+}$  was buffered to  $< 1$  nM (0 Ca). The pipette contained either 0 Ca ( $\circ$ , 9 vacuoles), or solutions with 5  $\mu M$  ( $\square$ , 3–5 vacuoles), 50  $\mu M$  ( $\blacksquare$ , 8 vacuoles), or 2 mM ( $\bullet$ , 5 vacuoles) free  $Ca^{2+}$ . The data for 0 and 2 mM  $Ca^{2+}$  are presented as mean  $\pm$  SD, while only means are given for 5  $\mu M$  and 50  $\mu M$   $Ca^{2+}$  inside the vacuole (SDs were in the same range as for 0 and 2 mM  $Ca^{2+}$ ). Solid lines are low-order polynomials fitted to the data. (b) The dependence of fast vacuolar currents on the vacuolar  $Ca^{2+}$  concentration. Experiments presented in (a), plus additional data for three separate vacuoles with 18  $\mu M$  free  $Ca^{2+}$  inside were analysed. Current amplitudes were measured at  $-100$  mV, normalised to 0  $Ca^{2+}$  and plotted as mean  $\pm$  SD. The data points were fitted by a Hill equation (solid line), yielding a Hill coefficient of  $0.512 \pm 0.030$  and  $\log(K_d) = -4.84 \pm 0.032$ , i.e.  $K_d = 14.4 \mu M$ .

binding, resulting in a Michaelis constant for  $K^+$  of  $K_m = 33.5 \pm 9.3$  mM and maximal conductance of  $23.8 \pm 1.5$  S  $m^{-2}$ . The slope conductance determined from the linear portion of the  $I / V$  relationships of the inward whole-vacuole current was  $33.2 \pm 1.9$  and  $40.5 \pm 6.9$  S  $m^{-2}$  for 100 and 1000 mM vacuolar  $K^+$ , respectively ( $n = 6$  and 4 vacuoles). The slope conductance was about twofold higher for the inward current compared with the outward current. An increase from 100 to 1000 mM on both sides of the vacuolar membrane resulted in a small increase (20 to 30%) of the measured currents, indicating comparable  $K^+$  affinities on both membrane sides (data not shown).

Under symmetrical ion conditions with 0  $Ca^{2+}$  and 100 mM KCl on both sides of the membrane, the  $I / V$  relationship of the whole-vacuole current was not linear but slightly asymmetrical. It displayed a characteristic high

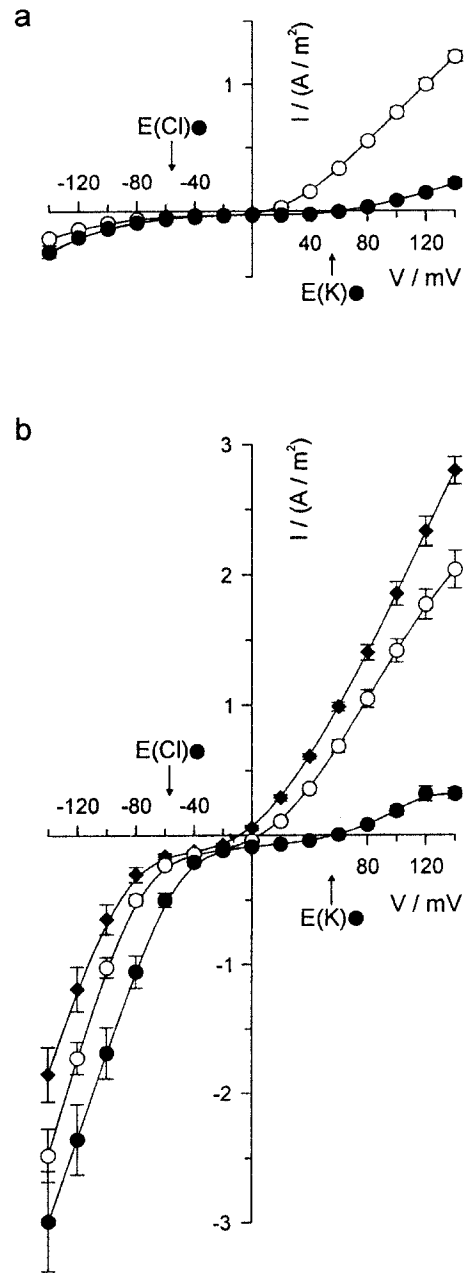


**Figure 4.** Fast vacuolar current is selective for  $K^+$  over  $Cl^-$ . (a) Whole vacuole  $I / V$  relationships measured at 0 Ca in the bath and 2 mM  $Ca^{2+}$  inside the vacuole. After measuring in symmetrical 100 mM KCl ( $\circ$ ), the bath was substituted by a 10 mM KCl solution ( $\bullet$ ). The current amplitudes from three vacuoles were normalized to the vacuolar membrane surface, averaged and expressed as means  $\pm$  SD in  $A m^{-2}$ . Arrows indicate the equilibrium potentials for  $K^+$  and  $Cl^-$  at a 10/100 mM KCl gradient across the vacuolar membrane. (b) Whole-vacuole  $I / V$  relationships measured at 0 Ca on both membrane sides. After measuring in symmetrical 100 mM KCl ( $\circ$ ), the bath was substituted by a 10 mM KCl solution ( $\bullet$ ) ( $n = 6$ ). With three vacuoles, the bath solution was further changed to 300 mM KCl ( $\blacklozenge$ ).

resistance region at about  $-40$  mV (Figures 2b, 3a and 4). This observation was consistently reproduced with more than 200 vacuoles. An increase of cytosolic  $K^+$  to 300 mM

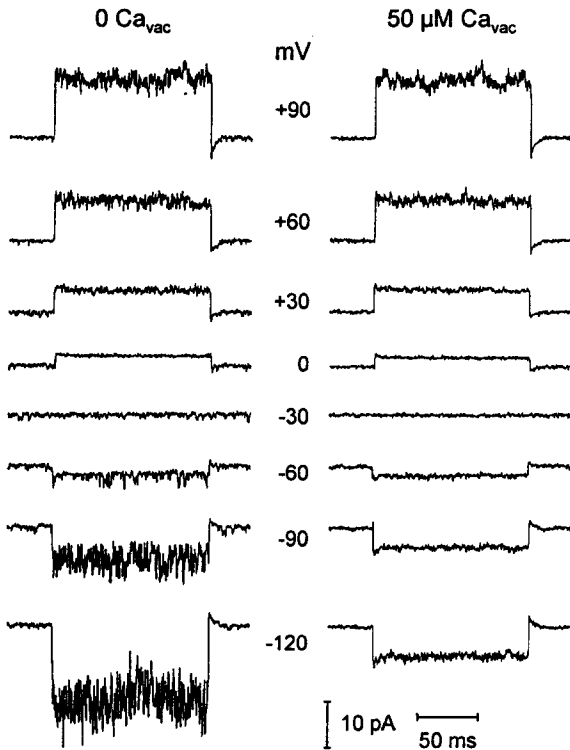


**Figure 5.** Fast-activating currents in excised vacuolar side-out membrane patches.

Instantaneous voltage-dependent activation and blockage by vacuolar calcium of current fluctuations in excised patches. From a holding potential of  $-30$  mV, steps of 130 ms duration were applied to voltages as indicated. The records were filtered at 2.5 kHz and sampled at 10 kHz. The currents on the left-hand side were measured at symmetrical 100 mM KCl, 0  $\text{Ca}^{2+}$ . On the right-hand side, the vacuolar free  $\text{Ca}^{2+}$  was 50  $\mu\text{M}$ . No leak subtraction was applied, the seal resistance was about 13 G $\Omega$ .

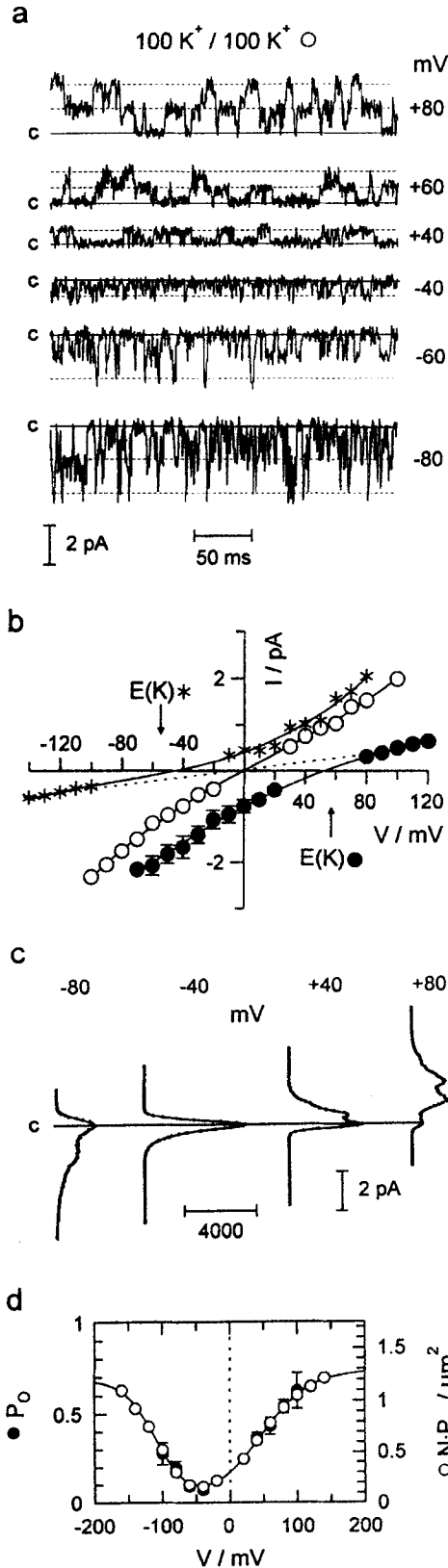
or its decrease to 10 mM resulted in approximately  $-20$  mV or  $+40$  mV shifts of this high resistance region (Figure 4). Thus, the high-resistance region was shifted in the same direction as the  $\text{K}^+$  equilibrium potential.

#### Identification of single ion channels responsible for the fast vacuolar current

Under conditions favouring observation of the fast-activating vacuolar current (low cytosolic  $\text{Ca}^{2+}$ ) using isolated vacuolar membrane patches ( $n = 117$ ), we recorded flickering voltage-dependent currents such as shown in Figure 5. At symmetrical ion conditions with 0  $\text{Ca}^{2+}$  on both membrane sides, current fluctuations were less frequent at small negative ( $-30$  mV) potentials, whereas at more negative and at positive voltages, their probability increased. The voltage-dependent transitions between low and high activity were very fast. We attempted to resolve their kinetics with six separate tonoplast patches, but the transitions occurred in less than a few milliseconds after application of the voltage step (Figure 5). Similarly to the whole-vacuole measurements, an increase of the vacuolar

free  $\text{Ca}^{2+}$  concentration to 50  $\mu\text{M}$ , by bath perfusion with a vacuolar side-out patch, caused an outward rectification of the fast-activating currents in isolated tonoplast patches (Figure 5). The flickering current at negative voltages was greatly reduced, almost to the leak current level, whereas current fluctuations at positive voltages were not affected.

Due to the high activity, the fast-activating currents in isolated membrane patches could often hardly be resolved at the single-channel level. To resolve single-channel currents at large negative and at positive potentials, recordings were performed with small patch pipettes (diameter  $< 1 \mu\text{m}$ ) to reduce the membrane surface of the patch. From long recordings, we selected short stretches with lower channel activity where the single-channel current amplitudes could be resolved for further analysis. Figure 6(a) shows single-channel activity recorded in this way from a cytoplasmic side-out patch bathed in symmetrical 100 mM KCl, 0  $\text{Ca}^{2+}$ . The first indication that the ion channel shown in Figure 6(a) shares the properties of the fast vacuolar current comes from its voltage dependence. At  $-40$  mV, only rare channel openings were observed, whereas at positive and more negative voltages, the activity increased. Single-channel currents displayed a slight outward rectification under symmetrical ion conditions, with a slope conductance of  $25.1 \pm 0.8$  pS and  $17.5 \pm 0.4$  pS ( $n = 14$  patches) at negative and positive potentials, respectively (Figure 6b, open circles). This partly explains the different slope conductance of the whole-vacuole current at positive and large negative potentials (Figure 4) but not the existence of the high-resistance region. The latter is obviously caused by the voltage-dependence of the single-channel open probability ( $P_o$ ) which was analysed as shown in Figure 6(c). All-points amplitude histograms of recordings lasting some seconds were fitted by a sum of Gaussian distributions. Assuming independent gating of FV channels, the equations describing a binomial distribution were introduced into the fit routine which reduced the number of fit parameters and yielded  $P_o$  as a fit parameter. With three active channels (in some patches only two), all histograms were perfectly described assuming a binomial distribution (Figure 6c), and the single-channel current amplitudes resulting from these fits were the same as those measured directly from the single channel traces.  $P_o$  had a minimum at  $-40$  mV. This was compared with the voltage-dependence of the average number of open channels in whole vacuoles ( $N \cdot P_o$ ) which was calculated by dividing whole-vacuole currents by single-channel currents.  $P_o$  and  $N \cdot P_o$  displayed exactly the same voltage-dependence (Figure 6d). This voltage-dependence was mathematically described assuming three states, one closed and two open, occupied at large negative and positive potentials (Figure 6d, solid line). The equilibrium between each open state and the closed one was



described by a Boltzmann distribution. This analysis yielded  $N = 1.75$  for the mean number of channels per  $\mu m^2$ .

To analyse the ion selectivity of the fast-activating vacuolar channels, we changed the bath solution with cytosolic side-out patches from 100 to 10 mM KCl, and repeated single-channel measurements under this 10/100 mM KCl gradient. The resulting  $I/V$  relationship is shown in Figure 6(b) (filled circles). The reversal potential of the single-channel current under a 10/100 mM KCl gradient was +50 mV which came close to the Nernst potential for  $K^+$ . This was in perfect agreement with reversal potential determinations in the whole-vacuole mode (Figure 4). Using the Goldman-Hodgkin-Katz equation, a relative  $K^+/Cl^-$  permeability of about 30 can be estimated from the reversal potential. Replacement of 100 mM KCl in the bath

**Figure 6.** Permeability and voltage-dependence of single channels.

(a) Single-channel activity of a cytosolic side-out patch in symmetrical 100 mM KCl, 0  $Ca^{2+}$  at different voltages. Single-channel traces were filtered at 1 kHz and sampled at 2.5 kHz. The closed state of the ion channels (c) is indicated by a solid line, and one or two open channels are indicated by dashed lines.

(b) Single-ion channels are selective for  $K^+$  over  $Cl^-$ . Single-channel current amplitudes measured in symmetrical 100 mM KCl were plotted as a function of the applied membrane potential ( $\circ$ ). Data points give the mean for six different patches (SD was smaller than the symbol size). With three cytoplasmic side-out patches, the bath solution was changed to 10 mM KCl solution ( $\bullet$ ). Data points are expressed as means  $\pm$  SD. With a single vacuolar side-out patch, the bath solution was changed to 10 mM KCl solution (\*). Solid lines are low-order polynomials fitted to the data. Linear regression analysis for data points at 10 mM vacuolar and cytosolic KCl is given by the dashed line, and a slope conductance of  $4.3 \pm 0.3$  pS was estimated. Equilibrium potentials for  $K^+$  ( $E(K)$ ) at 10/100 mM KCl (\*) and 100/10 mM KCl gradients ( $\bullet$ ) are indicated by arrows.

(c) All-points amplitude histograms indicating the number of sample points with a certain current amplitude (the horizontal bar corresponds to 4000 sample points) at four different voltages. The data are from the same experiment as the single-channel traces shown in (a). All-points amplitude histograms were fitted by a sum of Gaussian distributions assuming independent gating (solid line). With three active channels, this yielded  $P_o = 0.28 \pm 0.006$  at -80 mV,  $P_o = 0.13 \pm 0.01$  at -40 mV,  $P_o = 0.25 \pm 0.004$  at +40 mV, and  $P_o = 0.52 \pm 0.004$  at +80 mV. The closed state (c) is indicated by the horizontal solid line connecting all four histograms. Original records lasting 5 s were sampled at 10 kHz and filtered at 3 kHz.

(d) Comparison of the voltage-dependence of single channels and of whole vacuole currents in symmetrical 0  $Ca^{2+}$ , 100 mM KCl. The open probability of single channels ( $P_o$ ) from eight different excised membrane patches was analysed as shown in (c) and is given as means  $\pm$  SD ( $\bullet$ ). To calculate the voltage-dependence of whole-vacuole currents, whole-vacuole currents ( $n = 8$  separate vacuoles) were divided by the single-channel current at the corresponding voltage. These single-channel currents were taken from the mean single-channel  $I/V$  relationship of nine different patches fitted by a low-order polynomial. In this way, the average number of open channels per  $\mu m^2$  ( $\circ$ ) was calculated which corresponds to the open probability ( $P_o$ ) multiplied by the number of channels per  $\mu m^2$  ( $N$ ). The data for  $N \cdot P_o$  were fitted (solid line) assuming a bell-shaped voltage-dependence described by two Boltzmann functions. This yields  $1.07 \pm 0.08$  and  $0.70 \pm 0.02$  for the gating charges in the negative and positive potential ranges, respectively,  $-108 \pm 3$  mV and  $44 \pm 1$  mV for the midpoint potentials, and  $1.21 \pm 0.05$  and  $1.29 \pm 0.02 \mu m^{-2}$  for the maximum values of  $N \cdot P_o$  at negative and positive potentials, respectively. The data for  $P_o$  (single-channel open probability) were fitted by the same function divided by  $N$  taking the above parameters as constants. This single parameter fit yielded  $N = 1.75 \pm 0.06$  for the number of channels per  $\mu m^2$ .

by 10 mM KCl caused a shift of the voltage-dependence of the fast-activating vacuolar cation channel in a positive direction ( $n = 3$  patches). Now at  $-30$  mV, the activity was comparable to that observed at  $-80$  mV in symmetrical 100 mM KCl, and at  $+20$  mV only rare openings of single channels were observed (data not shown). This shift of the voltage-dependence upon changing the cytosolic  $K^+$  concentration was similar to that observed for the whole-vacuole current (Figure 4). The application of a 10/100 mM KCl gradient caused a rectification of the single-channel  $I/V$  relationship, the single-channel conductance at positive potentials decreased implying a smaller  $K^+$  efflux from the cytosolic side, whereas at negative potentials, the  $I/V$  relationship asymptotically approaches the  $I/V$  curve for symmetrical conditions (Figure 6b). An opposite rectification was observed with a vacuolar side-out patch when 100 mM KCl were replaced by 10 mM KCl (Figure 6b, asterisks). With this 100/10 mM KCl gradient, the reversal potential of the single channel current was about  $-50$  mV. This implies that the channel opening at negative and positive potentials, had the same  $K^+/Cl^-$  selectivity.

The single-channel conductance in 10 mM KCl was estimated from measurements with 10 mM KCl in the bath. Under these conditions, the outward current of cytosolic side-out patches and the inward currents of vacuolar side-out patches mainly reflected the  $K^+$  flow from the membrane side facing 10 mM KCl. Combining these two data sets, the single-channel conductance at 10 mM KCl can be estimated by linear regression (Figure 6b, dashed line). This results in a slope conductance of  $4.4 \pm 0.3$  pS. Compared with a value of 20.5 pS in symmetrical 100 mM KCl as an average for positive and negative potentials, this implies an increase of the single-channel conductance by a factor of 4.7 with a tenfold increase of the  $K^+$  concentration. This result is in good agreement with the increase of the outward whole-vacuole current, from 4.2 to 16.6  $S m^{-2}$ , for the same change of cytosolic  $K^+$  (Figure 4).

#### Cytosolic calcium inhibits the fast vacuolar channel

The effect of cytosolic  $Ca^{2+}$  on single-channel currents was measured in cytosolic side-out patches. A control measurement (Figure 7a, top) shows the single-channel activity at 0  $Ca^{2+}$  at both membrane sides. The bath was consecutively replaced by solutions containing 5 and 50  $\mu M$  free  $Ca^{2+}$  which resulted in a progressive decrease of single-channel activity (Figure 7a, lower traces). To give a quantitative description of the effect of cytosolic  $Ca^{2+}$ , we estimated the time-averaged channel-mediated current, which is the total time-averaged ion current across the membrane patch minus the leak current. The leak current is given by the level when all channels are closed. The data for six separate patches, normalized to the control at zero cytosolic  $Ca^{2+}$  are presented in Figure 7(b). It can be

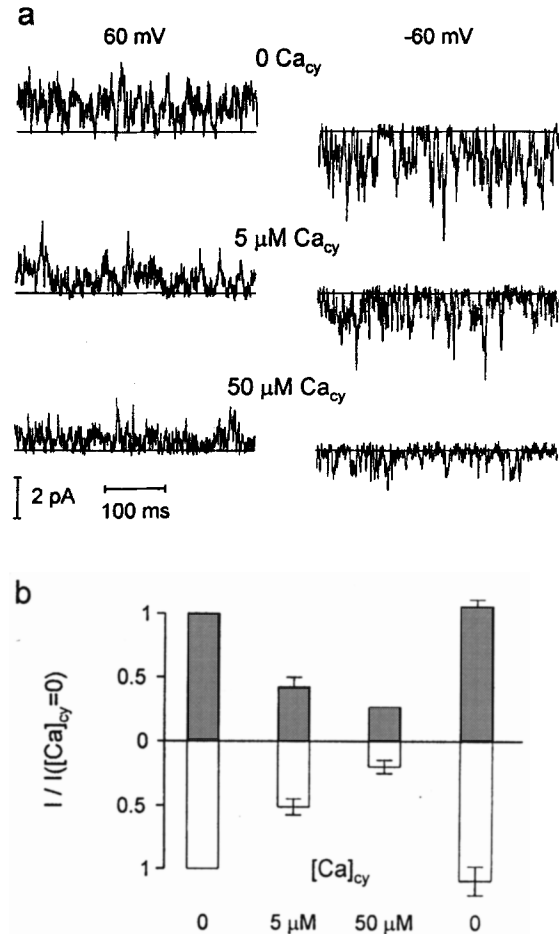


**Figure 7.** Cytosolic  $Ca^{2+}$  inhibits the single-channel activity, both at positive and negative membrane potentials.

(a) Activity of single fast-activating vacuolar channels at three different levels of cytosolic  $Ca^{2+}$ . Single-channel traces were recorded at  $+60$  and  $-60$  mV with a cytosolic side-out patch bathed in symmetrical 100 mM KCl, 0  $Ca$  (top traces). The free  $Ca^{2+}$  concentration at the cytoplasmic side (in the bath) was increased to 5  $\mu M$  (centre traces) and further to 50  $\mu M$  (lower traces). The patch contained several copies of fast-activating ion channels. The current level with no channels open is indicated by a solid horizontal line. The records were filtered at 500 Hz.

(b) The time-averaged single-channel current reversibly decreases with the increase of the cytosolic  $Ca^{2+}$  concentration. For 10 to 20 s of continuous recording at  $+60$  mV (upper black columns) or at  $-60$  mV (lower white columns), the time-averaged channel-mediated currents were calculated and normalized to 0  $Ca_{cy}$ . Mean currents for six separate cytosolic side-out patches at 5 and 50  $\mu M$  cytosolic  $Ca^{2+}$  are presented as means  $\pm$  SD. The column without an error bar at  $+60$  mV and 50  $\mu M$   $Ca^{2+}$  is the result of only one measurement. In all other patches the activity of some SV channels obscured the activity of fast vacuolar channels under these conditions. Single-channel activity was fully restored in all six patches when the 0  $Ca^{2+}$  solution was returned to the bath (right columns).

seen that an increase of the cytosolic free  $Ca^{2+}$  concentration caused a decrease of inward and outward currents by approximately 50% at 5  $\mu M$   $Ca^{2+}$  and by 75–80% at 50  $\mu M$   $Ca^{2+}$ . This is in good agreement with our whole-vacuole measurements where an increase of free cytosolic  $Ca^{2+}$  concentration caused a decrease of both outward and

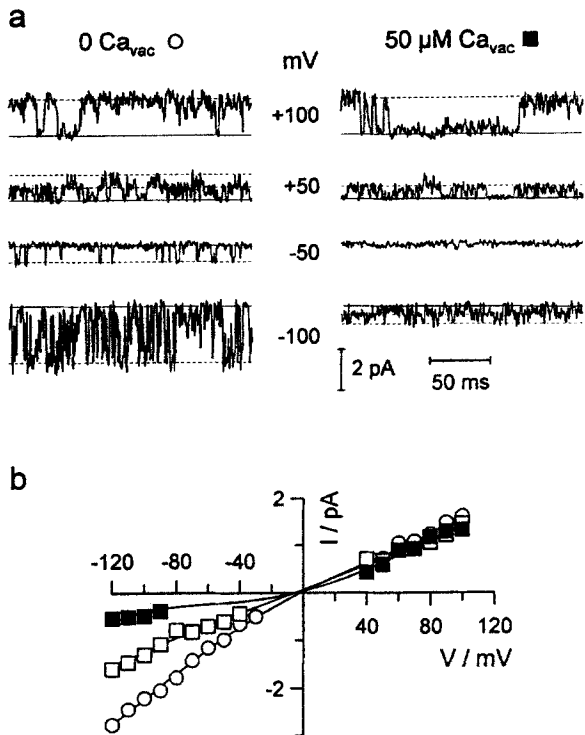


**Figure 8.** Vacuolar calcium blocks the outward current through fast-activating vacuolar channels.

(a) Single-channel traces of vacuolar side-out patches in symmetrical 100 mM KCl at four different membrane voltages (+100, +50, -50 and -100 mV). With 0  $\text{Ca}^{2+}$  in the pipette (cytosolic side), two different  $\text{Ca}^{2+}$  concentrations (0 and 50  $\mu\text{M}$ ) were perfused to the bath. The solid line indicates the current level with no channel open, the dashed lines indicate one or two open channels.

(b) Current-voltage relationship of the single-channel current at different levels of vacuolar  $\text{Ca}^{2+}$ . Single-channel current amplitudes were plotted as a function of membrane voltage at different vacuolar  $\text{Ca}^{2+}$ . For 0  $\text{Ca}_{\text{vac}}$  (○) and 50  $\mu\text{M}$   $\text{Ca}_{\text{vac}}$  (■), means of three different vacuolar side-out patches are given (SD was smaller than the symbol size). The amplitude at 5  $\mu\text{M}$  vacuolar  $\text{Ca}^{2+}$  (□) was measured once. Solid lines are low-order polynomials fitted to the data.

inward fast-activating currents by 50% at 5  $\mu\text{M}$   $\text{Ca}^{2+}$  and by 80% at 50  $\mu\text{M}$   $\text{Ca}^{2+}$  (Figure 2c). Reversibility of the inhibition by cytosolic  $\text{Ca}^{2+}$  was shown by returning to the 0  $\text{Ca}^{2+}$  solution at the end of the experiment.

#### Vacuolar calcium reduces the single-channel current

To analyse the effect of vacuolar  $\text{Ca}^{2+}$ , we performed measurements with vacuolar side-out patches. Again, control measurements were done at 0  $\text{Ca}^{2+}$  at both membrane sides. The single-channel traces and resulting  $I/V$  relationships are shown in Figure 8 (open circles). The replacement of the bath solution by a solution with 5  $\mu\text{M}$  free  $\text{Ca}^{2+}$  caused a decrease of single-channel current amplitudes at negative potentials (Figure 8b, open squares). At -100 mV, a decrease of 40% was measured. The whole-vacuole current was reduced by 35% under 5  $\mu\text{M}$  vacuolar  $\text{Ca}^{2+}$

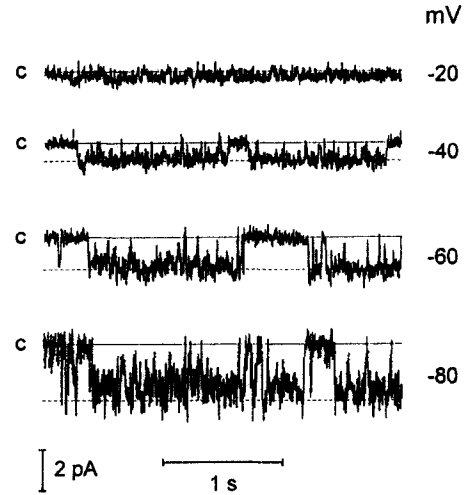


**Figure 9.** A voltage-independent ion channel.

Single-channel activity of a cytoplasmic side-out patch at four different membrane voltages (-20, -40, -60, and -80 mV) in symmetrical 100 mM KCl, 0  $\text{Ca}^{2+}$ . Data were filtered at 200 Hz and sampled at 500 Hz. The solid line indicates the current level with no channel open, the dashed line indicates one open channel.

(Figure 3). A bath solution with 50  $\mu\text{M}$  free  $\text{Ca}^{2+}$  caused a large decrease of single-channel currents at negative potentials, and at the same time the very rapid channel gating seemed to be slowed down, as shown in Figure 8 (filled squares). At -100 mV, a decrease of 78% was measured. The whole-vacuole current was reduced by 65% under these conditions (Figure 3). The single-channel currents at positive potentials were unaffected at up to 50  $\mu\text{M}$   $\text{Ca}^{2+}$  at the vacuolar side (Figure 8). A further increase of vacuolar  $\text{Ca}^{2+}$  to 2 mM resulted in completely 'silent' patches at negative voltages – only the leak current was recorded (data not shown). This was not surprising, as the whole-vacuole current under these conditions was decreased to about 5% of the control. At positive voltages, single-channel activity was slightly lower and single-channel currents decreased by about 20% to  $14.3 \pm 0.3$  pS ( $n = 6$ ) at 2 mM vacuolar  $\text{Ca}^{2+}$  (data not shown). This explains the observed 37% decrease of the whole-vacuole current at positive potentials with 2 mM  $\text{Ca}^{2+}$  in the vacuole compared with 0  $\text{Ca}^{2+}$  (Figure 3a).

In about 10% of all patches, the activity of another ion channel was observed, as depicted in Figure 9. This ion channel displayed slow kinetics, i.e. prolonged openings and closures, and had a single-channel conductance of about 30 pS (in 100 mM KCl). This channel was almost voltage-independent. Due to the infrequent appearance and short periods of channel activity, we were not able to examine this channel in more detail.

#### Discussion

Using the patch-clamp technique, we characterized the fast-activating currents in barley mesophyll vacuoles at

the whole-vacuole and the single-channel level. These instantaneously activating currents dominated at low cytosolic  $\text{Ca}^{2+}$ . In accordance with Hedrich and Neher (1987) who were the first to observe these currents in sugarbeet (*Beta vulgaris*) taproot vacuoles, we will call them FV currents (fast vacuolar) and the corresponding ion channel the FV channel.

#### Identification of the fast vacuolar ion channel (FV channel)

Both whole-vacuole and single-channel measurements showed a relative high selectivity for  $\text{K}^+$  over  $\text{Cl}^-$ ,  $P_{\text{K}}/P_{\text{Cl}} \approx 30$ , as shown in Figures 4 and 6. Although the FV channel binds  $\text{Ca}^{2+}$  with a high affinity from both membrane sides, there was no indication of a significant  $\text{Ca}^{2+}$  permeability. Even with large  $\text{Ca}^{2+}$  gradients, we never observed a shift of the reversal potential of whole-vacuole (compare Figures 1 and 2; Figure 4) or single-channel currents (Figures 7 and 8). The dependence of whole-vacuole and single-channel currents on  $\text{K}^+$  concentration yields a half-saturation at about 35 mM for inward and outward currents, indicating comparable binding affinities for  $\text{K}^+$  on both membrane sides.

The voltage-dependence of whole-vacuole and single-channel currents was exactly the same (Figure 6d). From comparison of the single-channel open probability ( $P_{\text{O}}$ ) and the average number of open channels in whole vacuoles ( $N \cdot P_{\text{O}}$ ), a density of nearly two FV channel per  $\mu\text{m}^2$  of vacuolar membrane was calculated. The characteristic high-resistance region at about 40 mV negative of the  $\text{K}^+$  equilibrium potential (Figure 4b) was explained by a minimum single-channel activity at the corresponding voltage (Figures 5 and 6). The FV channel appears to have at least one closed state (about 40 mV negative of  $E_{\text{K}}$ ) and two open states occupied at more positive and more negative potentials. At negative potentials, channel gating was significantly faster (shorter open times) compared with positive voltages (Figures 5 to 8). The two open states of the FV channel differed kinetically and by their unitary conductance. At the same time, they had equal  $\text{K}^+/\text{Cl}^-$  selectivities (Figure 5b).

Vacuolar  $\text{Ca}^{2+}$  blocked the FV channel in a voltage-dependent manner, i.e. an increase of the vacuolar  $\text{Ca}^{2+}$  concentration caused a larger decrease of the inward FV current compared with the outward FV current (Figure 3a and 8). The decrease of the inward FV current by vacuolar  $\text{Ca}^{2+}$  was described by a binding isotherm with a  $K_{\text{d}}$  of about 14  $\mu\text{M}$  (Figure 3b). At vacuolar  $\text{Ca}^{2+}$  activities in the millimolar range, a decrease of the outward FV current was observed (Figure 3).

Cytosolic  $\text{Ca}^{2+}$  blocked the FV channel in a voltage-independent manner (Figure 2 and 7), indicating a  $\text{Ca}^{2+}$ -binding site that is located close to the tonoplast surface.

The decrease of the FV current was described by a binding isotherm with a  $K_{\text{d}}$  of about 6  $\mu\text{M}$  for cytosolic free  $\text{Ca}^{2+}$  (Figure 2c). Inward and outward currents both at the whole-vacuole and at the single-channel level displayed the same sensitivity towards cytosolic  $\text{Ca}^{2+}$ , corroborating the view that the currents at positive and negative potentials are due to the same type of ion channel, the FV channel. In more than hundred tonoplast patches with 0  $\text{Ca}^{2+}$  inside the vacuole, we never observed FV channel activity only at negative or at positive potentials. Rather, the maximal numbers of simultaneously open FV channels at positive and at large negative membrane potentials always corresponded to each other (Figures 5 to 8), and inward and outward whole vacuole currents always had the same proportion (Figures 2b, 3a and 4).

Summarizing, the selectivity, voltage-dependence and  $\text{Ca}^{2+}$  sensitivity of the fast-activating whole-vacuole currents described here can be explained at the molecular level by the properties of a single calcium-inhibited cation-selective ion channel, namely the FV channel.

#### Comparison with other vacuolar channels

Hedrich and Neher (1987) were the first to describe the FV current. The whole-vacuole  $I/V$  relationship published by Hedrich and Neher (1987) showed a high-resistance region slightly negative of the  $\text{K}^+$  equilibrium potential similar to the  $I/V$  characteristic shown here (Figures 2–4). The fast-activating whole vacuole current in sugarbeet vacuoles was only observed at  $\text{Ca}^{2+}$  concentrations at the cytosolic side below 1  $\mu\text{M}$ , comparable to our results (Figures 1 and 2). The selectivity of the whole-vacuole FV current was not investigated by Hedrich and Neher (1987). Single-channel currents with a conductance of about 30 to 40 pS (in 200 mM KCl) and a cation over anion selectivity ( $P_{\text{K}}/P_{\text{Cl}}$ ) of about 6 were measured under low cytosolic  $\text{Ca}^{2+}$  in sugarbeet vacuoles (Hedrich and Neher, 1987). This channel seems to be different from the FV channel described here. It does not display an obvious voltage-dependence of the open probability, has a much lower cation over anion selectivity (6 compared to 30), a higher single-channel conductance and a much slower gating behaviour (Figures 5 and 6). The ion channel described by Hedrich and Neher (1987) is much more similar to the ion channel shown in Figure 9 which has a comparable conductance and gating behaviour. However, we do not think that this channel is responsible for the fast-activating whole-vacuole currents, as this channel was observed only rarely and did not display a significant voltage-dependence.

Colombo *et al.* (1989) observed instantaneously activating vacuolar currents in *Acer pseudoplatanus* cultured cells. At 1 mM  $\text{Ca}^{2+}$  inside the vacuole and 1  $\mu\text{M}$   $\text{Ca}^{2+}$  at the cytosolic side, these currents display a pronounced outward rectification (referring to the vacuolar side it is

called an inward rectification in the original publication), reminiscent of the fast-activating currents described here for barley. In contrast to the results of Hedrich and Neher (1987) and the results described here, Colombo *et al.* (1989) observed no effect of the cytosolic  $\text{Ca}^{2+}$  concentration on the fast-activating currents. Kolb *et al.* (1987) described single potassium channels in isolated barley mesophyll vacuoles with a conductance of 18 pS (250 mM KCl) with no  $\text{Ca}^{2+}$  added. Davies and Sanders (1995) reported a slight increase of instantaneous vacuolar currents at low cytosolic  $\text{Ca}^{2+}$  (< 500 nM) when 5 mM ATP were added. They argued that this ATP-activated current could provide a shunt conductance for the vacuolar  $\text{H}^{+}$ -ATPase.

The  $\text{K}^{+}$ -selective instantaneous current discovered in *Vicia faba* guard cells, called VK current (Ward and Schroeder, 1994), is activated by micromolar cytosolic  $\text{Ca}^{2+}$ . The VK channels reveal a more than threefold higher unitary conductance in symmetrical 100 mM KCl (70 pS for VK), compared with the FV channel. Furthermore, the instantaneous nature of the VK current is caused by its largely voltage-independent open probability (Ward and Schroeder, 1994): a constant proportion of VK channels are always open. In contrast, the FV current is clearly voltage-dependent (Figure 6d), and the instantaneous nature is due to a very rapid transition from low to high single channel activity (Figure 5). Therefore, FV and VK channels are clearly different from each other. In contrast to the VK channel, the channel presented in Figure 9 is not  $\text{Ca}^{2+}$ -activated and has a lower single-channel conductance.

Instantaneous currents across the vacuolar membrane of the unicellular green alga *Eremosphaera viridis* were interpreted to result from two different current components (Linz and Köhler, 1994): a voltage-independent component which was inhibited by increasing cytosolic  $\text{Ca}^{2+}$  concentrations but not by high vacuolar  $\text{Ca}^{2+}$  concentrations, and an outward-rectifying component which was not affected by cytosolic  $\text{Ca}^{2+}$ . Both components are clearly different from the FV current.

The FV channel differs from the SV channel by its much faster activation (Hedrich and Neher, 1987) and its  $\text{Ca}^{2+}$  dependence. Increasing cytosolic  $\text{Ca}^{2+}$  concentrations shift the voltage dependence of the SV channel to less positive voltages (Reifarth *et al.*, 1994; Schulz-Lessdorf and Hedrich, 1995), while the voltage-dependence of the FV channel was not shifted by cytosolic  $\text{Ca}^{2+}$  (Figures 1 and 2).

Although there are only very few reports about FV channels, we think that the FV channel is widespread in plant vacuoles. Using the experimental protocols and  $\text{Ca}^{2+}$ -buffered solutions described in this paper, we were able to resolve FV currents in mesophyll vacuoles from *Peperomia metallica* and rye (unpublished results). The unphysiologically high  $\text{Ca}^{2+}$  concentration at the cytosolic side used by many researchers is probably the reason why the FV

channel was not observed in most patch-clamp studies on plant vacuoles. This inhibition of the FV channel by high cytosolic  $\text{Ca}^{2+}$  may serve as an identification criterion for this vacuolar ion channel.

#### *Possible physiological role of the fast vacuolar channel*

At physiological cytosolic  $\text{Ca}^{2+}$  activities of 100–200 nM (Bush, 1995), the FV channel is expected to be active (Figures 1 and 2). Published values for vacuolar free  $\text{Ca}^{2+}$  concentrations range from 0.2 mM to 2.3 mM (Bethmann *et al.*, 1995; Felle, 1988; Miller and Sanders, 1987). Interestingly, in barley mesophyll cells, the vacuolar  $\text{Ca}^{2+}$  concentration is well regulated and kept constant at 1 to 2 mM when the  $\text{Ca}^{2+}$  concentration in the culture medium is changed 100-fold, from 0.3 to 30 mM (Dietz *et al.*, 1992). Although the inward current through the FV channels is largely suppressed by millimolar  $\text{Ca}^{2+}$  in the vacuole, it still remains in the range of some 10 pA at 2 mM vacuolar  $\text{Ca}^{2+}$  (Figure 3). Thus, at physiological conditions, the fast vacuolar channel plays the role of an outward-rectifying  $\text{K}^{+}$  channel which allows  $\text{K}^{+}$  efflux from the cytoplasm into the vacuole and to a lesser extent  $\text{K}^{+}$  influx from the vacuole into the cytoplasm.

If the FV channel gives rise to a high  $\text{K}^{+}$  permeability of the vacuolar membrane under physiological conditions, the electrical potential difference across the vacuolar membrane might come close to the equilibrium potential for  $\text{K}^{+}$ . Published data sets that include tonoplast potentials and  $\text{K}^{+}$  gradients seem to corroborate this view. In those cases where the measured tonoplast potential is vanishingly small, vacuolar and cytosolic  $\text{K}^{+}$  concentrations do not differ significantly (Bethmann *et al.*, 1995; Trebacz *et al.*, 1994). In those cases where negative tonoplast potentials were measured, ranging from –18 to –27 mV, the vacuolar  $\text{K}^{+}$  concentration is significantly smaller than the cytosolic one, and in each case the resulting driving force of the  $\text{K}^{+}$  gradient (+22 to +24 mV) nearly completely balances the electrical driving force (Raven, 1967; Rona *et al.*, 1982; Vorobiev, 1967). Thus, under physiological conditions, the tonoplast is likely to have a significant  $\text{K}^{+}$  permeability due to the activity of the FV channel, and this results in a tonoplast potential which is close to the equilibrium potential for  $\text{K}^{+}$ .

Keeping in mind the presence of different electrogenic transporters in the tonoplast, this high  $\text{K}^{+}$  permeability may be meaningful. There are two  $\text{H}^{+}$ -phosphohydrolases, namely the V-type  $\text{H}^{+}$ -ATPase and the pyrophosphatase which build up the  $\text{H}^{+}$  gradient across the tonoplast, and a large number of secondary transport systems which use the  $\text{H}^{+}$  gradient to transport other substances – such as anions, cations, sugars and amino acids – across the tonoplast (Martinoia, 1992; Taiz, 1992). Whenever the activity of these electrogenic transport systems is not perfectly

balanced, this gives rise to an increasing tonoplast potential which interferes with electrogenic transport processes. The FV channel clamps the tonoplast potential close to the equilibrium potential for  $K^+$  and thus prevents large changes of the tonoplast potential. As  $K^+$  is the most abundant cation in plant cells, with concentrations of 100–200 mM in the cytosol, the  $K^+$  fluxes needed to electrically compensate other transport processes are probably too small to cause large changes in the  $K^+$  gradient across the tonoplast.

### Conclusion

The FV channel is the only vacuolar ion channel identified to date that is highly selective for monovalent cations ( $K^+$ ), gated open at physiological  $Ca^{2+}$  activities and at physiological tonoplast potentials, and probably widespread in different plant cells. We propose that the FV channel is responsible for a high  $K^+$  permeability of the tonoplast clamping the tonoplast potential close to the equilibrium potential for  $K^+$ .

### Experimental procedures

#### Isolation of barley mesophyll protoplasts

Protoplasts were isolated from primary leaves of 7–9-day-old barley plants (*Hordeum vulgare* L.) grown under a 14 h 20°C light/10 h 18°C dark cycle. The preparation procedure was modified from Martinoia *et al.* (1981). The leaves were stripped from their abaxial epidermis and floated on the surface of 500 mM D-sorbitol, 1 mM  $CaCl_2$ , 15 mM Mes-Tris (pH 5.5), 0.1% BSA (Roth, Karlsruhe, Germany), 1% cellulase Y-C, 0.01% pectolyase Y-23 (both from Seishin Pharmaceutical, Tokyo, Japan) and 0.5% macerozyme R-10 (Serva, Darmstadt, Germany). After 1 h incubation at 30°C, the released protoplasts were filtered through a 0.5 mm nylon net, collected by centrifugation (20 min, 125 g) and purified by flotation (10 min, 1750 g) through a Percoll (Pharmacia, Upsala, Sweden) density gradient with (1) suspension of protoplasts in 500 mM sorbitol, 30 mM HEPES-Tris (pH 7.5), 30% Percoll; (2) 500 mM sorbitol, 0.8 mM  $CaCl_2$ , 12 mM MES plus 6 mM HEPES (pH 6.0 with Tris), 0.04% polyvinylpyrrolidone, 0.08% BSA, 20% Percoll; (3) 500 mM sorbitol, 1 mM  $CaCl_2$ , 15 mM MES-Tris (pH 5.5), 0.05% polyvinylpyrrolidone, 0.1% BSA. After centrifugation, the mesophyll protoplasts were collected from the interface between steps 2 and 3, and were kept on ice during the experiment.

#### Experimental solutions

The standard bath solution contained 100 mM KCl, 5 mM EGTA, 15 mM Tricine-Tris (pH 7.5). Osmolalities of this and all other solutions were adjusted to 650 mOsm with sorbitol and verified by a cryoscopic osmometer (Osmomat 030, Germany). Patch-clamp microelectrodes were filled either with the same solution as the bath, or, alternatively, by one containing 2 mM  $CaCl_2$  instead

of 5 mM EGTA. The basic solution for measurements of calcium dependence contained 100 mM KCl, 15 mM Tricine-Tris (pH 7.5), 2 mM EGTA (ethylene glycol bis( $\beta$ -aminoethyl)- $N,N,N',N'$ -tetraacetic acid), 2 mM HEDTA ( $N$ -(2-hydroxyethyl) ethylenediaminetetraacetic acid), 2 mM NTA (nitrilotriacetic acid), 400 mM sorbitol. Stability constants for complexes of different chelators with calcium were taken from Otto *et al.* (1985). Free calcium concentrations in the range of 1.4 nM to 490  $\mu$ M were adjusted by variable additions of  $CaCl_2$  to the basic solution. For calculations of free from total  $Ca^{2+}$  concentration, a home-made computer program was used (courtesy of Dr A. Alexeev, Pushchino). The total (resulting free)  $Ca^{2+}$  concentrations (in  $\mu$ M) were: 90 (0.0014), 550 (0.011), 1550 (0.077), 2600 (0.66), 3500 (2.9), 3700 (4.9), 4200 (12.7), 4350 (18.3), 4650 (30.4), 4750 (35.7), 4900 (48.6), 5300 (89.1), 5350 (104) and 6300 (493). Nominally  $Ca^{2+}$ -free basic solutions containing 100 mM KCl, 15 mM Tricine-Tris (pH 7.5), 2 mM EGTA, 2 mM HEDTA, 2 mM NTA, 400 mM sorbitol or 100 mM KCl, 15 mM Tricine-Tris (pH 7.5), 5 mM EGTA and 410 mM sorbitol were routinely measured by ICP-AES (ion-coupled plasma atomic emission spectroscopy). Total  $Ca^{2+}$  concentrations ranged from 3 to 10  $\mu$ M, which corresponds to free  $Ca^{2+}$  concentrations of 0.2 to 0.7 nM. Solutions without added  $Ca^{2+}$  containing < 1 nM free  $Ca^{2+}$  were referred to as 0  $Ca^{2+}$ .

#### Patch-clamp measurements and data analysis

A single vacuole was mechanically isolated from a protoplast within the measuring chamber. For this, a glass micro-electrode filled with the standard bath solution was attached to a protoplast and the plasma membrane was ruptured by application of a suction pulse. By this quick and simple procedure, a new vacuole was isolated for each measurement. Within a few minutes after the release of the vacuole, the patch-clamp measurement was initiated with a fresh glass micro-electrode.

Patch pipettes were made from Kimax-51 glass capillaries (Kimble Products, Vineland, NJ) using a two-step pulling protocol (electrode puller L/M-3P-A, List Medical, Darmstadt, Germany). The tip diameters of patch pipettes after fire-polishing were 2–3  $\mu$ m and about 1  $\mu$ m for whole-vacuole and single-channel measurements, respectively. When the electrodes were filled with the standard solution, this resulted in resistances of 2–5 M $\Omega$  and 10–15 M $\Omega$  for the two types of micro-electrodes. For high-resolution single channel recordings, the tip of the glass pipette was coated with silgarde (Silicones RTV615, General Electric Co., Watérford, NY).

After achievement of a high-resistance seal (10–20 G $\Omega$ ) of the patch pipette with the tonoplast, the measurements of vacuolar ion currents were performed under voltage-clamp conditions using one of three different geometries (Hamill *et al.*, 1981): whole-vacuole (analogous to whole-cell) cytosolic side-out excised patch (cytoplasmic side of the membrane faces the bath; technically an outside-out patch) and vacuolar side-out excised patch (vacuolar side faces the bath; technically an inside-out patch). Whole-vacuole measurements were started 20–30 min after rupturing the vacuolar membrane inside the pipette to ensure complete equilibration of the pipette solution with the interior of the vacuole. During this time, protoplast remains were completely washed away. The membrane capacitance of vacuoles used in this study was 7–28 pF, which corresponds to diameters between 15 and 30  $\mu$ m. The capacitance and the access resistance were monitored and compensated throughout the experiment and this compensation was controlled each time before an  $I/V$  curve was recorded. Measurements were performed under continuous bath perfusion

(5–10  $\mu\text{l s}^{-1}$ ). The solution volume in the experimental chamber was 0.1–0.15 ml.

The reference AgCl electrode was connected to the bath via a 3% agar bridge filled with 100 mM KCl. Current measurements were performed using an Axopatch 200A Integrating Patch-Clamp Amplifier (Axon Instruments, Foster City, CA). In this work, all bath and electrode solutions contained mainly KCl, so liquid junction potentials were negligible small (Barry and Lynch, 1991). The sign convention for current and voltage is according to Bertl *et al.* (1992), i.e. the sign of voltage refers to the cytosolic side, and positive (outward) currents represent an efflux of cations into the vacuole.

Records were filtered at 10 kHz by a low-pass Bessel filter, digitized using a VR-10B digital data recorder (Instrutech Corp., New York, NY) and stored on videotape. Whole-vacuole and single-channel currents were further filtered at 200–500 Hz and 0.5–2.5 kHz, respectively, and recorded directly on the hard disk of an IBM-compatible PC. The command voltage protocols were applied and analyses were carried out using the pClamp 6.0 software package (Axon Instruments, Foster City, CA). Data fitting was done with GRAFIT (Erithacus Software, London, U.K.) using a least-square fit routine based on the Marquardt algorithm.

### Acknowledgements

We thank Ms F. Reisberg and B. Hollenbach for skilful technical assistance. This work was funded by the Deutsche Forschungsgemeinschaft (SFB 176 TP33 and B11, Graduiertenkolleg GK-30360) and by a research fellowship from the Alexander von Humboldt Foundation to I.I.P.

### References

- Allen, G.J. and Sanders, D. (1995) Calcineurin, a type 2B protein phosphatase, modulates  $\text{Ca}^{2+}$ -permeable slow vacuolar ion channel of stomatal guard cells. *Plant Cell*, **7**, 1473–1483.
- Barry, P.H. and Lynch, W.J. (1991) Liquid junction potentials and small cell effects in patch-clamp analysis. *J. Membr. Biol.* **121**, 101–117.
- Bertl, A., Blumwald, E., Coronado, R. *et al.* (1992) Electrical measurements of endomembranes. *Science*, **258**, 873–874.
- Bethmann, B., Thaler, M., Simonis, W. and Schönknecht, G. (1995) Electrochemical potential gradients of  $\text{H}^+$ ,  $\text{K}^+$ ,  $\text{Ca}^{2+}$ , and  $\text{Cl}^-$  across the tonoplast of the green alga *Eremosphaera viridis*. *Plant Physiol.* **109**, 1317–1326.
- Bush, D.S. (1995) Calcium regulation in plant cells and its role in signaling. *Annu. Rev. Plant Physiol. Plant Mol. Biol.* **46**, 95–122.
- Colombo, R., Cerana, R., Lado, P. and Peres, A. (1989) Regulation by calcium of voltage-dependent tonoplast  $\text{K}^+$  channels. *Plant Physiol. Biochem.* **27**, 557–562.
- Davies, J.M. and Sanders, D. (1995) ATP, pH and  $\text{Mg}^{2+}$  modulate a cation current in *Beta vulgaris* vacuoles: a possible shunt conductance for the vacuolar  $\text{H}^+$ -ATPase. *J. Membr. Biol.* **145**, 75–86.
- Dietz, K.-J., Schramm, M., Lang, B., Lanzl-Schramm, A., Dürr, C. and Martinoja, E. (1992) Characterization of the epidermis from barley primary leaves. II. The role of the epidermis in ion compartmentation. *Planta*, **187**, 431–437.
- Felle, H. (1988) Cytoplasmic free calcium in *Riccia fluitans* L. and *Zea mays* L.: interaction of  $\text{Ca}^{2+}$  and pH? *Planta*, **176**, 248–255.
- Hamill, O.P., Marty, A., Neher, E., Sakmann, B. and Sigworth, F.J. (1981) Improved patch-clamp techniques for high-resolution current recording from cells and cell-free membrane patches. *Pflügers Arch. (Eur. J. Physiol.)* **391**, 85–100.
- Hedrich, R. and Neher, E. (1987) Cytoplasmic calcium regulates voltage-dependent ion channels in plant vacuoles. *Nature*, **329**, 833–835.
- Hedrich, R. and Kurkdjan, A. (1988) Characterization of an anion-permeable channel from sugar beet vacuole: effect of inhibitors. *EMBO J.* **7**, 3661–3666.
- Hedrich, R., Flügge, U.I. and Fernandez, J.M. (1986) Patch-clamp studies of ion transport in isolated plant vacuoles. *FEBS Lett.* **204**, 228–232.
- Hedrich, R., Barbier-Brygoo, H., Felle, H. *et al.* (1988) General mechanisms for solute transport across the tonoplast of plant vacuoles: a patch-clamp survey of ion channels and proton pumps. *Bot. Acta*, **107**, 7–13.
- Kolb, H.A., Köhler, K. and Martinoja, E. (1987) Single potassium channels in membranes of isolated mesophyll barley vacuoles. *J. Membr. Biol.* **95**, 163–170.
- Linz, K.W. and Köhler, K. (1994) Vacuolar ion currents in the primitive green alga *Eremosphaera viridis*: the electrical properties are suggestive of both the Characeae and higher plants. *Protoplasma*, **179**, 34–45.
- Martinoja, E. (1992) Transport processes in vacuoles of higher plants. *Bot. Acta*, **105**, 232–245.
- Martinoja, E., Heck, U. and Wiemken, A. (1981) Vacuoles as storage compartments for nitrate in barley leaves. *Nature*, **289**, 292–294.
- Miller, A.J. and Sanders, D. (1987) Depletion of cytosolic free calcium induced by photosynthesis. *Nature*, **326**, 397–400.
- Otto, M., May, P.M., Murray, K. and Thomas, J.D.R. (1985) Calibration of ionized calcium and magnesium with ligand mixtures for intracellular ion-selective electrode measurements. *Anal. Chem.* **57**, 1511–1517.
- Pantoja, O., Dainty, J. and Blumwald, E. (1992a) Cytoplasmic chloride regulates cation channels in the vacuolar membrane of plant cells. *J. Membr. Biol.* **125**, 219–229.
- Pantoja, O., Gelli, A. and Blumwald, E. (1992b) Voltage-dependent calcium channels in plant vacuoles. *Science*, **255**, 1567–1570.
- Raven, J.A. (1967) Ion transport in *Hydrodictyon africanum* J. *Gen. Physiol.* **50**, 1607–1625.
- Reifarth, W.F., Weiser, T. and Bentrup, F.-W. (1994) Voltage- and  $\text{Ca}^{2+}$ -dependence of the  $\text{K}^+$  channel in the vacuolar membrane of *Chenopodium rubrum* L. suspension cells. *Biochim. Biophys. Acta*, **1192**, 79–87.
- Rona, J.-P., Cornel, D., Grignon, C. and Heller, R. (1982) The electrical potential difference across the tonoplast of *Acer pseudoplatanus* cells. *Physiol. Veg.* **20**, 459–463.
- Schulz-Lessdorf, B. and Hedrich, R. (1995) Protons and calcium modulate SV-type channels in the vacuolar-lysosomal compartment. Channel interaction with calmodulin inhibitors. *Planta*, **197**, 655–671.
- Taiz, L. (1992) The plant vacuole. *J. Exp. Biol.* **172**, 113–122.
- Trebacz, K., Simonis, W. and Schönknecht, G. (1994) Cytoplasmic  $\text{Ca}^{2+}$ ,  $\text{K}^+$ ,  $\text{Cl}^-$ , and  $\text{NO}_3^-$  activities in the liverwort *Conocephalum conicum* L. at rest and during action potentials. *Plant Physiol.* **106**, 1073–1084.
- Vorobiev, L.N. (1967) Potassium ion activity in the cytoplasm and the vacuole of cells of *Chara* and *Griffithsia*. *Nature*, **216**, 1325–1327.
- Ward, J.M. and Schroeder, J.M. (1994) Calcium-activated  $\text{K}^+$  channels and calcium-induced calcium release by slow vacuolar ion channels in guard cell vacuoles implicated in the control of stomatal closure. *Plant Cell*, **6**, 669–683.
- Weiser, T. and Bentrup, F.-W. (1993) Pharmacology of the SV channel in the vacuolar membrane of *Chenopodium rubrum* suspension cells. *J. Membr. Biol.* **136**, 43–54.